SIAM J. SCI. COMPUT.
Vol. 25, No. 3, pp. 1018–1041

TWO-LEVEL FOURIER ANALYSIS OF A MULTIGRID APPROACH FOR DISCONTINUOUS GALERKIN DISCRETIZATION*

P. W. HEMKER†, W. HOFFMANN‡, AND M. H. VAN RAALTE†

Abstract. In this paper we study a multigrid (MG) method for the solution of a linear second order elliptic equation, discretized by discontinuous Galerkin (DG) methods, and we give a detailed analysis of the convergence for different block-relaxation strategies.

We find that pointwise block-partitioning gives much better results than the classical cellwise partitioning. Both for the Baumann–Oden method and for the symmetric DG method, with and without interior penalty (IP), the block-relaxation methods (Jacobi, Gauss–Seidel, and symmetric Gauss–Seidel) give excellent smoothing procedures in a classical MG setting. Independent of the mesh size, simple MG cycles give convergence factors of 0.075–0.4 per iteration sweep for the different discretization methods studied.

Key words. discontinuous Galerkin method, multigrid iteration, two-level Fourier analysis, pointwise block-relaxation

AMS subject classifications. 65F10, 65N12, 65N15, 65N30, 65N55

DOI. 10.1137/S1064827502405100

1. Introduction.

Although discontinuous Galerkin (DG) methods are traditionally used for the solution of hyperbolic equations [8, 17, 20], recently there has been renewed interest in their application to elliptic problems. Early methods for elliptic problems [9, 18] were considered unattractive because they resulted in discrete systems that showed saddle-point problem behavior. The nondefinite spectrum makes time-stepping procedures unstable and makes many iterative methods inadequate for the computation of steady solutions. This is fixed by introducing an interior penalty (IP) to penalize the discontinuity in the discrete solution [2, 21, 23], which is effective but leaves the user with the quite arbitrary choice of an $\mathcal{O}(h^{-1})$ penalty parameter.

In 1998 Oden, Babuška, and Baumann [19] (see also [5, 6]) published another stable method of DG type without such a free parameter. This interesting method, however, results in an asymmetric discrete operator, even for the discretization of a symmetric continuous problem. In this paper we consider the asymmetric (Baumann) and the symmetric discretization methods, both with and without IP. For an excellent survey and a unified analysis of the different DG methods for elliptic problems we refer to [3].

The motivation for our present research lies in our interest in the *hp*-self-adaptive solution of more general and three-dimensional problems on dyadic grids. Here DG methods are particularly attractive because of their ability to conveniently handle difficulties related to order- and grid-adaptation [16, 22]. For the solution of the resulting discrete systems we want to rely on multigrid (MG) methods because of their expected optimal efficiency. The framework of the combined adaptive discretization and the MG solution process is found, e.g., in [7, 13].

*Received by the editors April 8, 2002; accepted for publication (in revised form) February 27, 2003; published electronically November 21, 2003.
http://www.siam.org/journals/sisc/25-3/40510.html
†CWI, P.O. Box 94079, 1090 GB Amsterdam, The Netherlands (P.W.Hemker@cwi.nl, M.H.van.Raalte@cwi.nl) and KdV Institute for Mathematics, University of Amsterdam, Plantage Muidergracht 24, 1018 TV Amsterdam, The Netherlands (pieth@science.uva.nl, mvr@science.uva.nl).
‡KdV Institute for Mathematics, University of Amsterdam, Plantage Muidergracht 24, 1018 TV Amsterdam, The Netherlands (walter@science.uva.nl).

We emphasize that our approach is quite different from the analysis of MG as a preconditioner, analyzed for DG methods in [10]. Considering MG as an independent solution process gives us the opportunity not only to solve a linear system but also to simultaneously create the adaptive grid together with solving the discrete (linear) system. This use of MG allows us to drop the Krylov-space interation (as, e.g., conjugate gradient or GMRES), preserving the optimal $\mathcal{O}(N)$ property [11]. Moreover, the local mode analysis allows us to study not only the symmetric positive definite case but also the asymmetric and nonpenalized methods.

In this paper we study the convergence of the MG method by smoothing analysis and by analyzing the two-level convergence behavior, restricting ourselves to the discretized Poisson equation in one space dimension. With considerably extra complexity a similar analysis can be made for two or three space dimensions. In a forthcoming paper for the two-dimensional case [15] we show that, using the same techniques as used in this paper, but with proper modifications for more dimensions, again an efficient MG method can be constructed.

In this paper we show that the discrete operator can be partitioned in block-tridiagonal form in two essentially different ways: *cellwise* and *pointwise*. For each of these partitionings, block-relaxation methods (block-Jacobi, block-Gauss–Seidel) can be used as smoothing procedures in the MG algorithm. It appears that the type of block-partitioning makes an essential difference: the pointwise block-partitioning shows a much better convergence than the usual cellwise block-partitioning. It appears that pointwise block-partitioning even leads to good smoothing for the symmetric DG method of saddle-point type.

The outline of this paper is as follows. In section 2 we describe the DG discretizations used. We select a particular basis in the space of piecewise polynomial functions for the test and trial spaces in order to introduce the distinction between cellwise and pointwise block-partitionings. We introduce the MG algorithm and describe in detail the grid-transition operators used.

In section 3 we develop the Fourier analysis tools needed to make the local mode analysis for the block-Toeplitz matrices: the discretization operator, the prolongation, and the restriction operator. Then, in section 4 we apply the smoothing analysis to the cellwise and pointwise partitioned discretizations. We determine the smoothing factors and compute optimal damping parameters. The results motivate us to continue with the two-level analysis for the pointwise partitioning exclusively. Therefore, in section 5 we take the MG coarse-grid correction into account. We compute the spectral radii for the error reduction operators. It appears that an error reduction factor of 0.075 (for symmetric Gauss–Seidel (SGS)) to 0.4 (for damped Jacobi) per MG-sweep is predicted for the nonpenalized discretizations. For the penalized method the convergence is somewhat slower, but still faster than 0.6 per MG-sweep. In order to see what can be the worst possible behavior in a single as well as a couple of iteration sweeps, we also compute the corresponding spectral norms. We conclude that, for pointwise smoothers, MG converges rapidly in all cases.

In section 6 we show by Fourier analysis the consistency and the convergence of the discretization stencils obtained by the DG methods. This gives some additional insight into the accuracy of the different methods and the lack of adjoint consistency of Baumann's method as indicated in [3]. In the final section we show some numerical results that illustrate the analyzed behavior and show the fast convergence of the MG method.

2. The DG discretization.

2.1. DG methods. In order to describe the discretization method studied in this paper, we first give the special weak form of the equation as used for these DG discretization methods. On an open cube Ω, with boundary $\partial\Omega = \Gamma_D \cup \Gamma_N$, we consider the Poisson equation, partly with Neumann and partly with Dirichlet boundary conditions:

$$-\nabla \cdot \nabla u = f \text{ on } \Omega; \quad u = u_0 \text{ on } \Gamma_{\mathrm{D}} \cap \partial\Omega, \quad u_n = g \text{ on } \Gamma_N \cap \partial\Omega.$$

On Ω we introduce a uniform partitioning Ω_h, i.e., a set of disjoint rectangular, open cells Ω_e in Ω, all of identical shape:

$$\Omega_h = \left\{ \Omega_e \;\middle|\; \cup_e \overline{\Omega}_e = \overline{\Omega},\ \Omega_i \cap \Omega_j = \emptyset,\ i \neq j \right\}.$$

We define on Ω_h the *broken Sobolev space* [6, 19, 4] for nonnegative integer k,

$$H^k(\Omega_h) = \left\{ u \in L_2(\Omega) \;\middle|\; u|_{\Omega_e} \in H^k(\Omega_e) \quad \forall \Omega_e \in \Omega_h \right\}.$$

Then, the weak form of the equation, associated with the DG methods, reads as follows [6, 19]: Find $u \in H^1(\Omega_h)$ such that

$$B(u,v) = L(v) \quad \forall v \in H^1(\Omega_h), \tag{2.1}$$

where

$$\begin{aligned} B(u,v) = &\sum_{\Omega_e \in \Omega_h} \int_{\Omega_e} \nabla u \cdot \nabla v dx - \int_{\Gamma_{\mathrm{int}} \cup \Gamma_{\mathrm{D}}} \langle \nabla u \rangle \cdot [v]\, ds \\ &+ \sigma \int_{\Gamma_{\mathrm{int}} \cup \Gamma_{\mathrm{D}}} \langle \nabla v \rangle \cdot [u]\, ds + \mu \int_{\Gamma_{\mathrm{int}} \cup \Gamma_{\mathrm{D}}} [u] \cdot [v]\, ds \end{aligned} \tag{2.2}$$

and

$$L(v) = \sum_{\Omega_e \in \Omega_h} \int_{\Omega_e} fv\ dx + \sigma \int_{\Gamma_{\mathrm{D}}} \langle \nabla v \rangle \cdot [u_0]\, ds + \int_{\Gamma_N} gv\ ds.$$

Here Γ_{int} is the union of all interior cell faces, and $\sigma \neq 0$ and $\mu \geq 0$ are parameters identifying the different DG methods. ($\sigma = 1$ for Baumann's method; $\sigma = -1$ for symmetric DG; $\mu > 0$ is the IP parameter.) The jump operator $[\,\cdot\,]$ and the average operator $\langle \cdot \rangle$ are defined at the common interface $\Gamma_{i,j}$ between two adjacent[1] cells Ω_i and Ω_j by

$$\begin{aligned} [w(x)] &= w(x)|_{\partial\Omega_i} \mathbf{n}_i + w(x)|_{\partial\Omega_j} \mathbf{n}_j, \\ \langle w(x) \rangle &= \frac{1}{2} \left(w(x)|_{\partial\Omega_i} + w(x)|_{\partial\Omega_j} \right) \end{aligned} \tag{2.3}$$

for $x \in \Gamma_{i,j} \subset \Gamma_{\mathrm{int}}$. Here $\mathbf{n}_i$ is the unit outward pointing normal for cell Ω_i. In the case of a vector valued function, τ, we define

$$\begin{aligned} [\tau(x)] &= \tau(x)|_{\partial\Omega_i} \cdot \mathbf{n}_i + \tau(x)|_{\partial\Omega_j} \cdot \mathbf{n}_j, \\ \langle \tau(x) \rangle &= \frac{1}{2} \left(\tau(x)|_{\partial\Omega_i} + \tau(x)|_{\partial\Omega_j} \right). \end{aligned} \tag{2.4}$$

[1] At a Dirichlet boundary the interface with a virtual (flat, exterior) adjacent cell, containing only the Dirichlet data, is used.

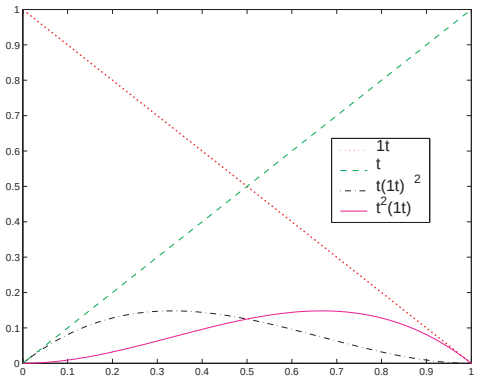

FIG. 1. $\phi_{n,k}(t) = t^{n+k}(1-t)^{n+1-k}$, $n = \{0,1\}$, $k = \{0,1\}$.

The DG discretization is obtained by specifying the finite-dimensional trial and test space $S_h \subset H^1(\Omega_h)$ as the space of piecewise polynomials of degree less than $2p$ on the partitioning Ω_h:

$$S_h = \left\{ \phi_{i,e} \in P^{2p-1}(\Omega_e), \quad \Omega_e \in \Omega_h \right\} .$$

Notice that we restrict ourselves to odd degree $k = 2p-1$. The discrete equations now read as follows: Find $u_h \in S_h$ such that

$$B(u_h, v_h) = L(v_h) \qquad \forall v_h \in S_h . \tag{2.5}$$

2.2. Choice of a basis. To completely describe the discrete matrix obtained, we should provide S_h with a basis. Therefore we introduce the following basis polynomials on the one-dimensional unit interval:

$$\phi_{2n+k}(t) = t^{n+k}(1-t)^{n+1-k}, \quad n = 0, 1, \ldots, p-1, \quad k = 0, 1. \tag{2.6}$$

On the unit cube, $\hat{\Omega} \subset \mathbb{R}^d$, we use a basis of tensor-product polynomials based on (2.6). A basis for $P^{2p-1}(\Omega_e)$ is obtained by the usual affine mapping $\widehat{\Omega} \to \Omega_e$.

The basis thus obtained has two advantages. First, it is hierarchical. This means that we can (locally) increase the accuracy of the approximation just by extending the basis with higher order polynomials. Second, the coefficients of the first degree polynomials represent function values at the cell-corners, while the coefficients of the polynomials of degree 3 can be associated with corrections for the derivatives at the cell-corners. All higher order polynomials, $\phi_{n,k}$, $n \geq 2$, are genuine bubble functions and correspond to interior cell corrections only.

A slightly better alternative basis satisfying our purposes is, defined on $[-1, +1]$, the basis $(x-1)^p(x+1)^q$ for $(p,q) = (1,0)$, $(0,1)$, $(2,1)$, $(1,2)$, and $(x-1)^2(x+1)^2 P_n^{(4,4)}(x)$ with $n = 0, 1, \ldots$, and $P_n^{(4,4)}$ the Jacobi polynomials [1, p. 774]. The first four polynomials in this basis are essential for our purpose because they represent function values and first derivatives at the cell boundaries. These are the same as in (2.6) for $p \leq 2$. The new, higher order polynomials satisfy the useful L_2-orthogonality property. This basis also relieves the restriction to odd degree k for $k > 3$.

If we are interested in fast convergence of the solution procedure for the discrete system, the coefficients for the bubble functions are of less importance because they

can be eliminated by static condensation or dealt with by defect correction. Therefore, in our analysis in the following sections we restrict ourselves to the case $p = 2$, in which the above two alternatives coincide. Furthermore, we restrict ourselves to the one-dimensional equation because this is the building block for the higher-dimensional case, where we essentially use tensor-product polynomials.

Using the basis $\{\phi_i\}_{i=0}^3$, the approximate solution reads

$$u_h = \sum_{e=1}^{N}\sum_{i=0}^{3} c_{i,e}\phi_i((x-x_e)/h) \equiv \sum_{e=1}^{N}\sum_{i=0}^{3} c_{i,e}\phi_{i,e}(x),$$

and we obtain the explicit form of the discrete system, $L_h u_h = f_h$,

$$\begin{aligned}(2.7)\qquad &\sum_{e=1}^{N}\sum_{i=0}^{3} c_{i,e}\left(\int_{\Omega_e}\phi'_{i,e}(x)\phi'_{j,e}(x)dx - \left\langle\phi'_{i,e}(x)\right\rangle\cdot[\phi_{j,e}(x)]\,|_{\Gamma_{\mathrm{Dint}}}\right.\\ &\qquad\left.+\,\sigma\,[\phi_{i,e}(x)]\cdot\left\langle\phi'_{j,e}(x)\right\rangle|_{\Gamma_{\mathrm{Dint}}} + \mu\,[\phi_{i,e}(x)]\cdot[\phi_{j,e}(x)]\,|_{\Gamma_{\mathrm{Dint}}}\right)\\ &= \sum_{e=1}^{N}\sum_{i=0}^{3}\int_{\Omega_e} f\phi_{j,e}(x)dx + \sigma\,[u_0]\cdot\left\langle\phi'_{j,e}(x)\right\rangle|_{\Gamma_{\mathrm{D}}} + g\phi_{j,e}(x)|_{\Gamma_N}\end{aligned}$$

for $4N$ test functions $\phi_{j,e}$. As usual, the resulting one-dimensional discrete operator has a block-tridiagonal structure. We want to emphasize that for solving this discrete system by block-relaxation we can follow two distinct approaches. The usual approach is to order the basis functions *cellwise*. Then the choice of a particular basis for the polynomial space is of less importance and the variables in each block are associated with the coefficients of the polynomial approximation in the corresponding cell. The other approach is by ordering the coefficients *pointwise* and to associate with each point the left- and right-sided values of the function and its derivative. (In fact, this motivates the particular choice of our basis (2.6).)

Ordering the equations (the weighting functions $\phi_{e,j}$) and coefficients *cellwise* as $[c_{e,0}, c_{e,2}, c_{e,3}, c_{e,1}]$ yields the following discretization stencil:

(2.8)
$$\left[\begin{array}{cccc|cccc|cccc}
-\frac{1}{2} & 0 & -\frac{1}{2} & \frac{1-\sigma}{2}-h\mu & \frac{1+\sigma}{2}+h\mu & \frac{1}{2} & 0 & \frac{-1-\sigma}{2} & \frac{1}{2}\sigma & 0 & 0 & 0\\
0 & 0 & 0 & \frac{1}{2}\sigma & -\frac{1}{2}\sigma & \frac{2}{15} & \frac{1}{30} & 0 & 0 & 0 & 0 & 0\\
0 & 0 & 0 & 0 & 0 & \frac{1}{30} & \frac{2}{15} & -\frac{1}{2}\sigma & \frac{1}{2}\sigma & 0 & 0 & 0\\
0 & 0 & 0 & \frac{1}{2}\sigma & \frac{-1-\sigma}{2} & 0 & \frac{1}{2} & \frac{1+\sigma}{2}+h\mu & \frac{1-\sigma}{2}-h\mu & -\frac{1}{2} & 0 & -\frac{1}{2}
\end{array}\right].$$

If we order the equations and coefficients *pointwise*, according to function values and corrections on derivatives at the cell-interfaces, $[c_{e-1,3}, c_{e-1,1}, c_{e,0}, c_{e,2}]$, we get the stencil

$$(2.9)\qquad \left[\begin{array}{cccc|cccc|cccc}
0 & 0 & 0 & \frac{1}{30} & \frac{2}{15} & -\frac{1}{2}\sigma & \frac{1}{2}\sigma & 0 & 0 & 0 & 0 & 0\\
0 & \frac{1}{2}\sigma & \frac{-1-\sigma}{2} & 0 & \frac{1}{2} & \frac{1+\sigma}{2}+h\mu & \frac{1-\sigma}{2}-h\mu & -\frac{1}{2} & 0 & -\frac{1}{2} & 0 & 0\\
0 & 0 & -\frac{1}{2} & 0 & -\frac{1}{2} & \frac{1-\sigma}{2}-h\mu & \frac{1+\sigma}{2}+h\mu & \frac{1}{2} & 0 & \frac{-1-\sigma}{2} & \frac{1}{2}\sigma & 0\\
0 & 0 & 0 & 0 & 0 & \frac{1}{2}\sigma & -\frac{1}{2}\sigma & \frac{2}{15} & \frac{1}{30} & 0 & 0 & 0
\end{array}\right].$$

For the Poisson equation on the uniform grid, in both cases the discretization matrix appears to be a block-Toeplitz matrix. This matrix is described by the repetition of either stencil (2.8) or stencil (2.9).

2.3. The MG algorithm. Our main interest lies in the application of the DG method in the *hp*-self-adaptive MG algorithm. Therefore we use an adaptive MG algorithm [13], where local refinements yield corrections for the coarser discretizations. In the linear case, if the total grid is refined, the *hp*-adaptive algorithm corresponds to the classical MG [11], combined with nested iteration. Its convergence is best studied by means of the two-level algorithm (TLA). The amplification operator of the error is given by

$$M_h^{\mathrm{TLA}} = (M_h^{\mathrm{REL}})^{\nu_2} M_h^{\mathrm{CGC}} (M_h^{\mathrm{REL}})^{\nu_1} , \tag{2.10}$$

ν_1 and ν_2 are the number of pre- (post-) relaxation sweeps, respectively, and

$$M_h^{\mathrm{CGC}} = I_h - P_{hH} L_H^{-1} \overline{R}_{Hh} L_h .$$

To each of the amplification operators of the error, M_h, corresponds an amplification operator for the residue $\overline{M}_h = L_h M_h L_h^{-1}$. In our analysis we are mainly interested in the convergence of the two-level iteration. Therefore we compute the spectral radius of the amplification operator $\rho(M_h^{\mathrm{TLA}}) = \rho(\overline{M}_h^{\mathrm{TLA}})$, which represents the final convergence factor per iteration step. We also compute the spectral norms $\|(M_h^{\mathrm{TLA}})^t\|_2$ and $\|(\overline{M}_h^{\mathrm{TLA}})^t\|_2$, which describe the worst possible convergence rate in t steps.

2.4. Restrictions and prolongations. As we are interested in MG methods for the solution of the discrete equations arising from DG discretization, we need proper restriction and prolongation operators. With piecewise polynomial approximations on the separate cells of the partitioning Ω_h, a natural prolongation is immediately derived. For convenience we describe the grid transition operators for the one-dimensional case. Extension to higher dimensions follows immediately by means of the tensor-product principle.

We consider a fine partitioning Ω_h and a coarse partitioning Ω_H, with $H = 2h$ and with nodal points jh and jH, respectively, and we denote the spaces of discontinuous piecewise polynomials by S_h and S_H. It is immediately clear that $S_H \subset S_h$. This defines the natural prolongation $P_{hH} : S_H \to S_h$ so that $(P_{hH} u_H)(x) = u_H(x)$ for all $x \in \mathbb{R} \setminus \mathbb{Z}_h$.[2] Given a polynomial basis, this prolongation is explicitly described by its stencil. For our basis $\{\phi_{i,e}\}$ the stencil reads

$$P_{hH} \approxeq \left[\begin{array}{cccc|cccc|cccc|cccc|cccc}
0 & 0 & 0 & \frac{-1}{8} & 0 & 0 & 0 & \frac{1}{4} & \frac{3}{8} & 0 & 0 & 0 & 0 & 0 & 0 & 0 & 0 & 0 & 0 & 0 \\
0 & 0 & 0 & 0 & 0 & 0 & \frac{1}{2} & \frac{1}{8} & 0 & 1 & 0 & 0 & \frac{1}{8} & \frac{1}{2} & 0 & 0 & 0 & 0 & 0 & 0 \\
0 & 0 & 0 & 0 & 0 & 0 & \frac{1}{2} & \frac{1}{8} & 0 & 0 & 1 & 0 & \frac{1}{8} & \frac{1}{2} & 0 & 0 & 0 & 0 & 0 & 0 \\
0 & 0 & 0 & 0 & 0 & 0 & 0 & 0 & 0 & 0 & 0 & \frac{3}{8} & \frac{1}{4} & 0 & 0 & 0 & \frac{-1}{8} & 0 & 0 & 0
\end{array}\right] .$$

Different from the prolongation, a natural restriction is not uniquely determined. However, we recognize a natural restriction for the residue, associated with the weighted-residual character of the Galerkin discretization. This restriction is the adjoint of the natural prolongation; i.e., the Toeplitz operator for this restriction is the transpose of the Toeplitz operator for the natural prolongation. We denote this restriction as $\overline{R}_{Hh} = (P_{hH})^T$. It follows from the Galerkin construction of the discretization and from the nesting of the spaces S_h and S_H that the Galerkin relation exists between the discretization on the coarse grid and the finer grid,

$$L_H = \overline{R}_{Hh} L_h P_{hH} . \tag{2.11}$$

[2] $\mathbb{Z}_h$ is the infinite regular one-dimensional grid, defined by $\mathbb{Z}_h = \{jh \,|\, j \in \mathbb{Z}, h > 0\}$.

For the chosen basis $\{\phi_{i,e}\}$, which is essentially based on the function values and corrections for the derivatives at the cell endpoints, we can construct another pointwise restriction (the injective restriction). This restriction is constructed such that

$$\begin{aligned}(d/dx)(R_{Hh}u_h)(jH)|_{\Omega_{H,j-1}} &= (d/dx)u_h(2jh)|_{\Omega_{h,2j-1}}\,,\\ (R_{Hh}u_h)(jH)|_{\Omega_{H,j-1}} &= u_h(2jh)|_{\Omega_{h,2j-1}}\,,\\ (R_{Hh}u_h)(jH)|_{\Omega_{H,j}} &= u_h(2jh)|_{\Omega_{h,2j}}\,,\\ (d/dx)(R_{Hh}u_h)(jH)|_{\Omega_{H,j}} &= (d/dx)u_h(2jh)|_{\Omega_{h,2j}}\,.\end{aligned}$$

The stencil related to this restriction reads

$$R_{Hh} \approxeq \left[\begin{array}{cccc|cccc|cccc|cccc|cccc} 0&0&0&1&0&0&0&0&3&0&0&0&0&0&0&0&0&0&0&0\\ 0&0&0&0&0&0&0&0&0&1&0&0&0&0&0&0&0&0&0&0\\ 0&0&0&0&0&0&0&0&0&0&1&0&0&0&0&0&0&0&0&0\\ 0&0&0&0&0&0&0&0&0&0&0&3&0&0&0&0&1&0&0&0 \end{array}\right].$$

We see that the prolongation P_{hH} and this restriction R_{Hh} satisfy the relation $R_{Hh}P_{hH} = I_H$, i.e., the identity operator on S_H. This implies that the operator $P_{hH}R_{Hh}$ is a projection operator from S_h into itself. Its image, $\mathrm{Range}(P_{hH}) \subset S_h$, comprises the *fine grid functions representable* on the coarse grid. The range of the complementary projection $I_h - P_{hH}R_{Hh}$ is the set of *fine grid functions* that are *not representable* on the coarse grid.

3. Fourier analysis tools.

3.1. Fourier analysis for vector grid functions. In order to apply Fourier analysis methods for the convergence study of our solution process, we introduce some elementary tools. We first introduce (vector valued) grid functions defined on the regular, unbounded, one-dimensional grid $\mathbb{Z}_h = \{jh \,|\, j \in \mathbb{Z}, h > 0\}$.

The Hilbert space of square summable scalar grid functions, defined on $\mathbb{Z}_h$, with inner product $(u_h, v_h) = \sum_j\ h\ u_h(jh)v_h(jh)$, is denoted by $\ell^2(\mathbb{Z}_h)$. We will use the Fourier transform $\widehat{u_h}$ of $u_h \in l_h^2(\mathbb{Z}_h)$, which is the complex function defined on $\mathbb{T}_h = [-\pi/h, +\pi/h]$, defined by

$$\widehat{u_h}(\omega) = \frac{h}{\sqrt{2\pi}} \sum_{j\in\mathbb{Z}} e^{-ijh\omega}\, u_h(jh)\,. \tag{3.1}$$

We see that the function $\widehat{u_h}(\omega)$ is $(2\pi/h)$-periodic and that by Parseval's equality we have

$$\|u_h\|_{\ell^2(\mathbb{Z}_h)} = \|\widehat{u_h}\|_{L^2(\mathbb{T}_h)}\,. \tag{3.2}$$

In an obvious manner we can extend this definition of the Fourier transform $\ell^2(\mathbb{Z}_h) \to L^2(\mathbb{T}_h)$ to the Fourier transform of a four-dimensional vector function $\mathbf{u}_h \in \left[\ell^2(\mathbb{Z}_h)\right]^4 \to \widehat{\mathbf{u}_h} \in \left[L^2(\mathbb{T}_h)\right]^4$.

The transform (3.1), its inverse, as well as Parseval's equality (3.2), also hold if we replace u_h by the vector valued grid function $\mathbf{u}_h \in \left[\ell^2(\mathbb{Z}_h)\right]^4$ and $\widehat{u_h}$ by $\widehat{\mathbf{u}_h} \in \left[L^2(\mathbb{T}_h)\right]^4$, provided that we use the corresponding norms for the vector spaces

$$\|\mathbf{u}_h\|^2_{[\ell^2(\mathbb{Z}_h)]^4} = \sum_{i=1}^4 \|u_{h,i}\|^2_{\ell^2(\mathbb{Z}_h)} \qquad \text{and} \qquad \|\widehat{\mathbf{u}_h}\|^2_{[L^2(\mathbb{T}_h)]^4} = \sum_{i=1}^4 \|\widehat{u_{h,i}}\|^2_{\mathbb{T}_h}. \tag{3.3}$$

We apply this to the vector grid functions of coefficients, either for the cell-centered (*cellwise*) coefficients $u_h = \{[c_{e,0}, c_{e,2}, c_{e,3}, c_{e,1}]^T\}_{e\in\mathbb{Z}}$ or for the cell-corner (*pointwise*) coefficients $u_h = \{[c_{e-1,3}, c_{e-1,1}, c_{e,0}, c_{e,2}]^T\}_{e\in\mathbb{Z}}$. Cellwise vector grid functions are obtained from $H^2(\Omega_h)$ functions, with $\Omega = \mathbb{R}$, by the restriction operator $R^{\text{cell}}_{h,0} : H^2(\mathbb{R}_h) \to [\ell^2(\mathbb{Z}_h)]^4$ defined by

(3.4)
$$\mathbf{u}_h(jh) = (R^{\text{cell}}_{h,0}u)(jh) = \begin{bmatrix} & u((j-1)h)|_{\Omega_j} \\ h & u'((j-1)h)|_{\Omega_j} + u((j-1)h)|_{\Omega_j} - u(jh)|_{\Omega_j} \\ -h & u'(jh)|_{\Omega_j} - u((j-1)h)|_{\Omega_j} + u(jh)|_{\Omega_j} \\ & u(jh)|_{\Omega_j} \end{bmatrix},$$

where $u(jh)|_{\Omega_i}$ is the function value in grid point jh for the function u restricted to cell Ω_i. Pointwise vector grid functions are obtained by a restriction operator $R_{h,0} : H^2(\mathbb{R}_h) \to [\ell^2(\mathbb{Z}_h)]^4$ defined by

(3.5)
$$\mathbf{u}_h(jh) = (R_{h,0}u)(jh) = \begin{bmatrix} -h & u'(jh)|_{\Omega_{j-1}} - u\left((j-1)h\right)|_{\Omega_{j-1}} + u(jh)|_{\Omega_{j-1}} \\ & u(jh)|_{\Omega_{j-1}} \\ & u(jh)|_{\Omega_j} \\ h & u'(jh)|_{\Omega_j} + u(jh)|_{\Omega_j} - u\left((j+1)h\right)|_{\Omega_j} \end{bmatrix}.$$

In both cases the restriction determines the function values and the correction for the derivatives at the cell boundaries. Only the ordering in the vector function is different: the discrete data are either cellwise or pointwise collected. These two representations correspond to the representations (2.8) and (2.9) of the block-Toeplitz matrix obtained for the DG discretization.

3.2. Fourier analysis for a block-Toeplitz operator. For a block-Toeplitz matrix of the type as encountered in section 2.2 we can compute the Fourier transform and the eigenvalues as follows. Let $A_h = (\mathbf{a}_{m,j}) \in \mathbb{R}^{4\mathbb{Z}\times 4\mathbb{Z}}$ be an infinite Toeplitz operator, i.e., an operator with a block structure $\mathbf{a}_{m,j} \in \mathbb{R}^{4\times 4}$, $m, j \in \mathbb{Z}$, satisfying $\mathbf{a}_{m,m+k} = \mathbf{a}_{-k}$ for all $m, k \in \mathbb{Z}$, and let $e_{h,\omega}$ be an elementary mode, i.e., a complex function defined on the grid $\mathbb{Z}_h$ with $e_{h,\omega}(jh) = e^{ijh\omega}$. Then

$$\begin{aligned} &\sum_{j\in\mathbb{Z}} \mathbf{a}_{m,j} e_{h,\omega}(jh) = \widehat{A}_h(\omega) e_{h,\omega}(mh) \\ &\Leftrightarrow \widehat{A}_h(\omega) = \sum_{j\in\mathbb{Z}} \mathbf{a}_{m,j} e^{i(j-m)h\omega} = \sum_{k\in\mathbb{Z}} \mathbf{a}_{-k} e^{ikh\omega} = \sum_{k\in\mathbb{Z}} \mathbf{a}_k e^{-ikh\omega} \end{aligned} \tag{3.6}$$

for all $\omega \in \mathbb{T}_h \equiv [-\frac{\pi}{h}, \frac{\pi}{h}]$.

Now, let $V_h \in \mathbb{R}^{4\mathbb{Z}\times 4\mathbb{Z}}$ be an arbitrary diagonal block-Toeplitz matrix, with blocks $\mathbf{v}_{j,j} = \mathbf{v} \in \mathbb{R}^{4\times 4}$ for all $j \in \mathbb{Z}$. Then

$$\left(A_h V_h e_{h,\omega}\right)(mh) = \sum_{j\in\mathbb{Z}} \mathbf{a}_{m,j}\mathbf{v}_{j,j} e^{ijh\omega} = \left(\sum_{j\in\mathbb{Z}} \mathbf{a}_{m,j} e^{ijh\omega}\right)\mathbf{v} = \widehat{A}_h(\omega) e^{imh\omega}\mathbf{v}\,,$$

with $\widehat{A}_h(\omega) = \sum_{j\in\mathbb{Z}} \mathbf{a}_j e^{-ijh\omega}$. If we choose $\mathbf{v} = \mathbf{v}(\omega)$ to be the matrix of eigenvectors of $\widehat{A}_h(\omega)$ such that

$$\widehat{A}_h(\omega)\mathbf{v} = \mathbf{v}\Lambda_h(\omega), \tag{3.7}$$

then we have

$$(A_h V_h e_{h,\omega})(mh) = \widehat{A}_h(\omega)\mathbf{v}e_{h,\omega}(mh) = e_{h,\omega}(mh)\mathbf{v}\Lambda_h(\omega). \tag{3.8}$$

Hence, the columns of $\mathbf{v}(\omega)e_{h,\omega}(mh)$ are the eigenvectors of A_h. Also $\Lambda_h(\omega)$ is a family of 4×4 diagonal matrices with the eigenvalues of A_h at the diagonal entries.

COROLLARY. *The spectrum of the block-Toeplitz operator A_h is found as $\{\lambda_i(\omega)\}_{i=1,\dots,4}$, $\omega\in\mathbb{T}_h$, where $\lambda_i(\omega)$ is an eigenvalue of $\widehat{A_h}(\omega)$.*

3.3. Fourier analysis for prolongations and restrictions. Key to the Fourier analysis of prolongations and restrictions are the flat prolongation and restriction operators $P^0_{hH} : [\ell^2(\mathbb{Z}_H)]^4 \to [\ell^2(\mathbb{Z}_h)]^4$ and $R^0_{Hh} : \ell^2(\mathbb{Z}_h) \to \ell^2(\mathbb{Z}_H)$ that are defined by

$$\mathbf{u}_h(jh) = \left(P^0_{hH}\mathbf{u}_H\right)(jh) = \begin{cases} \mathbf{u}_H(Hj/2) & \text{if } j \text{ even} \\ \mathbf{0} & \text{if } j \text{ odd} \end{cases} \tag{3.9}$$

and

$$\left(R^0_{Hh}\mathbf{u}_h\right)(jH) = \mathbf{u}_h(2jh). \tag{3.10}$$

General, arbitrary constant coefficient prolongations (restrictions) can be constructed as a combination of a Toeplitz operator and a flat operator. Any prolongation P_{hH} can be written as $P_{hH} = P_h P^0_{hH}$ and any restriction R_{Hh} can be written as $R_{Hh} = R^0_{Hh}R_h$, with P_h (or R_h) a Toeplitz operator $[\ell^2(\mathbb{Z}_h)]^4 \to [\ell^2(\mathbb{Z}_h)]^4$.

A simple computation [12] shows

$$\widehat{P^0_{hH}\mathbf{u}_H}(\omega) = \frac{1}{2}\widehat{\mathbf{u}_H}(\omega), \quad \omega\in\mathbb{T}_h, \tag{3.11}$$

(notice the periodicity of $\widehat{u_H}(\omega)$ with period π/h !) and

$$\widehat{R^0_{Hh}\mathbf{u}_h}(\omega) = \sum_{p=0,1} \widehat{\mathbf{u}_h}\left(\omega + \frac{\pi p}{h}\right) \quad \forall\omega\in T_H = T_{2h}. \tag{3.12}$$

Here we see that $\widehat{P_{hH}u_H}$ is defined on $\mathbb{T}_h = [-\pi/h, +\pi/h]$, whereas $\widehat{u_H}$ is defined on the smaller $\mathbb{T}_H = [-\pi/2h, \pi/2h]$. This motivates us to introduce a different notation for the same Fourier transform $\widehat{v_h}(\omega)$, with $\omega\in\mathbb{T}_h$. We introduce the new notation

$$\begin{pmatrix} \widehat{v_h}(\omega) \\ \widehat{v_h}(\omega+\pi/h) \end{pmatrix}, \quad \omega\in\mathbb{T}_H\ ,$$

with exactly the same meaning as $\widehat{v_h}$, $\omega\in\mathbb{T}_h$.

Having introduced this notation, we may write (3.11) as

$$\widehat{P_{hH}\mathbf{u}_H}(\omega) = \left(P_h\widehat{P^0_{hH}\mathbf{u}_H}\right)(\omega) = \frac{1}{2}\begin{bmatrix} \widehat{P_h}(\omega) \\ \widehat{P_h}\left(\omega+\frac{\pi}{h}\right) \end{bmatrix}\widehat{\mathbf{u}_h}(\omega), \quad \omega\in\mathbb{T}_H, \tag{3.13}$$

and (3.10) as

$$\widehat{R_{Hh}\mathbf{u}_h}(\omega) = \widehat{R^0_{Hh}R_h}\mathbf{u}_h(\omega) = \begin{bmatrix} \widehat{R_h}(\omega), & \widehat{R_h}\left(\omega+\frac{\pi}{h}\right) \end{bmatrix}\begin{bmatrix} \widehat{\mathbf{u}_h}(\omega) \\ \widehat{\mathbf{u}_h}\left(\omega+\frac{\pi}{h}\right) \end{bmatrix}, \tag{3.14}$$

with $\omega\in\mathbb{T}_H$.

3.4. Filtering the true high frequency functions. On the one hand, we can define low and high frequency grid functions in $\ell^2(\mathbb{Z}_h)$ as the functions that are linear combinations of modes $e^{ijh\omega}$ with, respectively, $\omega \in \mathbb{T}_{2h}$ and $\omega \in \mathbb{T}_h \setminus \mathbb{T}_{2h}$. On the other hand, having introduced a prolongation P_{hH} and a restriction R_{Hh} in the solution space S_h, we may define low frequency components in the error as those components that lie in the range of the projection $P_{hH}R_{Hh}$, and high frequency components as the complementary functions, i.e., those in the range of $I_h - P_{hH}R_{Hh}$. In view of the MG algorithm, the latter approach is more relevant.

Since a low frequency grid function can be represented on the coarser grid, we obtain this grid function by considering a "slowly varying" (4-valued) grid function $\mathbf{u}_h$,

$$P_{hH}R_{Hh}\mathbf{u}_h = P_h P^0_{hH} R^0_{Hh} R_h \mathbf{u}_h. \tag{3.15}$$

Since $P_{hH}R_{Hh}$ is a projection, we have for a high frequency grid function $\mathbf{u}_h$:

$$(I - P_h P^0_{hH} R^0_{Hh} R_h)\mathbf{u}_h = \mathbf{u}_h\,. \tag{3.16}$$

In view of this we want our MG smoothers (the relaxation methods) to damp the contributions (3.16). In other words, those eigenvalues of the amplification operator M_h^{REL} that correspond to high frequency contributions (3.16) must be small. So we are interested in whether the eigenvalues are small for

$$\mathbf{FT}\left((I - P_h P^0_{hH} R^0_{Hh} R_h)\; M^{\mathrm{REL}}\right)(\omega), \quad \omega \in T_H\,, \tag{3.17}$$

where **FT** denotes the Fourier transform.

3.5. Fourier transform of the two-level operator. Now, with these tools available, we write, for the amplification operator of the coarse-grid correction operator

$$M_h^{\mathrm{CGC}} = I_h - P_{hH} L_H^{-1} \overline{R}_{Hh} L_h,$$

its Fourier transform

$$\widehat{M_h^{\mathrm{CGC}}}(\omega) = \left(\widehat{I_h} - \widehat{P_{hH}}\,\widehat{L_H^{-1}}\,\widehat{\overline{R}_{Hh}}\,\widehat{L_h}\right)(\omega) = \begin{pmatrix} 1 & 0 \\ 0 & 1 \end{pmatrix}$$
$$- \begin{pmatrix} \widehat{P_h}(\omega) \\ \widehat{P_h}(\omega + \pi/h) \end{pmatrix} (\widehat{L_H}(\omega))^{-1} \begin{pmatrix} \widehat{R_h}(\omega) & \widehat{R_h}(\omega + \pi/h) \end{pmatrix} \begin{pmatrix} \widehat{L_h}(\omega) & 0 \\ 0 & \widehat{L_h}(\omega + \pi/h) \end{pmatrix}.$$

In view of Parseval's equality (3.2) the eigenvalues of the 8×8-matrix $\widehat{M_h^{\mathrm{CGC}}}(\omega)$ for $\omega \in \mathbb{T}_H$ yield the eigenvalues of the coarse-grid correction operator M_h^{CGC} and, similarly, $\widehat{M_h^{\mathrm{TLA}}}(\omega) = (\widehat{M_h^{\mathrm{REL}}}(\omega))^{\nu_2}\widehat{M_h^{\mathrm{CGC}}}(\omega)(\widehat{M_h^{\mathrm{REL}}}(\omega))^{\nu_1}$ yield the eigenvalues for the two-level operator M_h^{TLA}.

4. Smoothing analysis. One of the main ingredients of an MG solver is the smoother. It is used to damp the high frequencies of the error on the finer grid, while the low frequency errors are damped by the coarse-grid correction. For this, the smoother should have an amplification operator with a proper eigenvalue spectrum. That is, an eigenvalue spectrum in which most eigenvalues are in absolute value less than one, where the larger eigenvalues correspond to low frequency eigenfunctions. In this section we apply Fourier analysis to study the amplification operator of the damped block-Jacobi (JOR) and the damped block-Gauss–Seidel (DGS) relaxation for

TABLE 1
The relaxation methods using $\alpha > 0$ as the relaxation parameter.

	B_h	M_h^{REL}
JOR	αD^{-1}	$D^{-1}((1-\alpha)D - \alpha(L+U))$
DGS_L	$\alpha(D+L)^{-1}$	$(D+L)^{-1}((1-\alpha)(D+L) - \alpha U)$
DGS_U	$\alpha(D+U)^{-1}$	$(D+U)^{-1}((1-\alpha)(D+U) - \alpha L)$

TABLE 2
The stencils in the diagonal decomposition.

Cellwise		Pointwise
$\begin{bmatrix} -\frac{1}{2} & 0 & -\frac{1}{2} & \frac{1-\sigma}{2} - h\mu \\ 0 & 0 & 0 & \frac{1}{2}\sigma \\ 0 & 0 & 0 & 0 \\ 0 & 0 & 0 & \frac{1}{2}\sigma \end{bmatrix}$	L	$\begin{bmatrix} 0 & 0 & 0 & \frac{1}{30} \\ 0 & \frac{1}{2}\sigma & \frac{-1-\sigma}{2} & 0 \\ 0 & 0 & -\frac{1}{2} & 0 \\ 0 & 0 & 0 & 0 \end{bmatrix}$
$\begin{bmatrix} \frac{1+\sigma}{2} + h\mu & \frac{1}{2} & 0 & \frac{-1-\sigma}{2} \\ -\frac{1}{2}\sigma & \frac{2}{15} & \frac{1}{30} & 0 \\ 0 & \frac{1}{30} & \frac{2}{15} & -\frac{1}{2}\sigma \\ \frac{-1-\sigma}{2} & 0 & \frac{1}{2} & \frac{1+\sigma}{2} + h\mu \end{bmatrix}$	D	$\begin{bmatrix} \frac{2}{15} & -\frac{1}{2}\sigma & \frac{1}{2}\sigma & 0 \\ \frac{1}{2} & \frac{1+\sigma}{2} + h\mu & \frac{1-\sigma}{2} - h\mu & -\frac{1}{2} \\ -\frac{1}{2} & \frac{1-\sigma}{2} - h\mu & \frac{1+\sigma}{2} + h\mu & \frac{1}{2} \\ 0 & \frac{1}{2}\sigma & -\frac{1}{2}\sigma & \frac{2}{15} \end{bmatrix}$
$\begin{bmatrix} \frac{1}{2}\sigma & 0 & 0 & 0 \\ 0 & 0 & 0 & 0 \\ \frac{1}{2}\sigma & 0 & 0 & 0 \\ \frac{1-\sigma}{2} - h\mu & -\frac{1}{2} & 0 & -\frac{1}{2} \end{bmatrix}$	U	$\begin{bmatrix} 0 & 0 & 0 & 0 \\ 0 & -\frac{1}{2} & 0 & 0 \\ 0 & \frac{-1-\sigma}{2} & \frac{1}{2}\sigma & 0 \\ \frac{1}{30} & 0 & 0 & 0 \end{bmatrix}$

both stencils (2.8) and (2.9). So, we distinguish between cellwise block- and pointwise block-relaxations.

We will observe that with cellwise relaxations the amplification operators have a complex eigenvalue spectrum with many eigenvalues close to one. This indicates that this relaxation shows a poor and oscillating convergence. However, for pointwise block-relaxations the amplification operators show much better spectra.

For the discrete system $A_h x = b$ we consider the iterative process

$$x^{(i+1)} = x^{(i)} - B_h(A_h x^{(i)} - b)\,, \tag{4.1}$$

with B_h an approximate inverse of A_h. Decomposing A_h as

$$A_h = L + D + U, \tag{4.2}$$

into a strict block-lower, block-diagonal; and strict block-upper matrix, the different relaxation methods are uniquely described either by B_h or by the amplification matrix $M_h^{\mathrm{REL}} = I_h - B_h A_h$. These operators are shown in Table 1. Because A_h is a block-Toeplitz operator, the amplification matrix M_h also is block-Toeplitz. Notice that the meaning of the block decomposition (4.2) is different for stencils (2.8) and (2.9). The stencils corresponding to the decomposition $A_h = (\mathbf{a}_{m,j})$ are given in Table 2.

The difference between cellwise and pointwise block decomposition is that the eigenvectors $e_{h,\omega}(mh)\mathbf{v}$ of the cellwise stencil correspond to 4-valued grid functions associated with the cell interiors (in fact independent of the chosen basis), whereas for

the pointwise stencil, they correspond to the 4-valued grid function (3.5) associated with *the nodal points* between the cells. This makes the cellwise stencil less suited for an MG algorithm because it is less natural to define prolongations and restrictions for the staggered information than from the pointwise information in coarse and fine cells.

Using (3.6) we find the Fourier transforms of the basic Toeplitz operators:

$$\widehat{L}(\omega) = L\, e^{-i\omega h}, \quad \widehat{D}(\omega) = D, \quad \widehat{U}(\omega) = U\, e^{i\omega h}. \tag{4.3}$$

This yields the Fourier transform for the amplification operators of JOR and DGS:

$$\widehat{M_{JOR}^{REL}} = \widehat{D}^{-1}\left((1-\alpha)\,\widehat{D} - \alpha\,\left(\widehat{L}+\widehat{U}\right)\right),$$

$$\widehat{M_{DGS_L}^{REL}} = \left(\widehat{D}+\widehat{L}\right)^{-1}\left((1-\alpha)\left(\widehat{D}+\widehat{L}\right) - \alpha\,\widehat{U}\right),$$

$$\widehat{M_{DGS_U}^{REL}} = \left(\widehat{D}+\widehat{U}\right)^{-1}\left((1-\alpha)\left(\widehat{D}+\widehat{U}\right) - \alpha\,\widehat{L}\right).$$

Because of (3.8), computing the eigenvalues of $\widehat{M_h^{REL}}(\omega)$ for $\omega \in \mathbb{T}_h$ we find the eigenvalues of M_h^{REL}. The eigenvalues corresponding to the high frequencies (i.e., the frequencies $|\omega| > \pi/2h$ that cannot be represented on the coarser grid) are found to be $\widehat{M_h^{REL}}(\omega)$ for $\omega \in \mathbb{T}_h \setminus \mathbb{T}_H$. For the various DG methods, viz., for Baumann's method, $\sigma = 1$, $\mu = 0$; for the symmetric DG method, $\sigma = -1$, $\mu = 0$; and for the IP DG method, $\sigma = -1$, $\mu = C/h$, Figures 2–10 show the eigenvalue spectra of JOR, DGS, and SGS relaxation amplification operators, the last amplification operator being defined by $M_{SGS}^{REL} = M_{DGS_L}^{REL} M_{DGS_U}^{REL}$.

We notice that the spectra of the amplification operators *for pointwise ordering* of the block-relaxations appear to be the same for the Baumann and symmetric DG methods ($\sigma = 1$ or $\sigma = -1$).

Although in the figures we distinguish between the behavior of low and high frequencies (LF: $|\omega| < \pi/2h$ and HF: $|\omega| \geq \pi/2h$), this does not precisely correspond to the meaning of LF and HF in the context of MG. Typical LF components in an MG algorithm are those functions that are invariant under the projection $P_{hH}R_{Hh}$ (they are in the range of the prolongation), whereas the HF components are those in the kernel of the restriction. Therefore, we take into account the properties of the restriction and prolongation to determine optimal relaxation parameters and also determine the spectra of the operator $M^{\mathrm{REL}}(I_h - P_{hH}R_{Hh})$.

Because Figures 2–10 show clearly that the convergence behavior for pointwise relaxation is much better than for cellwise relaxation, we further restrict our study to the former.

Figures 11–13 show the spectra of the operator $M^{\mathrm{REL}}(I_h - P_{hH}R_{Hh})$, again applied to the three different types of DG methods. From these results we can determine optimal damping parameters for relaxation. This parameter, minimizing the spectral radius $\rho(M_h^{REL}(I_h - P_{hH}R_{Hh}))$ is given by

$$\alpha_{opt} = \frac{2}{2 - (\lambda_{\min} + \lambda_{\max})},$$

where $\lambda_{\min}$ and $\lambda_{\max}$ are, respectively, the minimum and maximum (real) eigenvalues of the spectrum without damping. The damping parameters are given in Table 3.

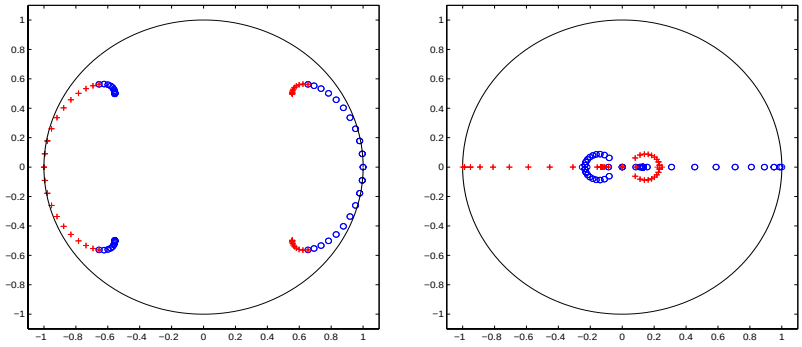

FIG. 2. *Eigenvalue spectra of* $\widehat{M^{REL}_{JOR}(\omega)}$ *for Baumann's DG method (without damping:* $\sigma = 1$, $\mu = 0$, $\alpha = 1$*) relative to the unit circle.*

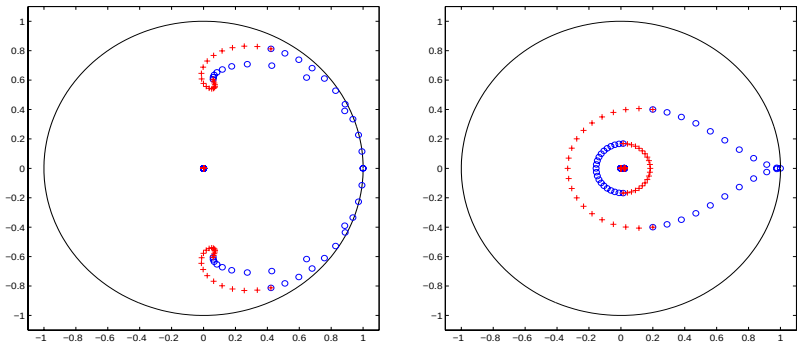

FIG. 3. *Eigenvalue spectra of* $\widehat{M^{REL}_{DGS}(\omega)}$ *for Baumann's DG method (without damping:* $\sigma = 1$, $\mu = 0$, $\alpha = 1$*) relative to the unit circle.*

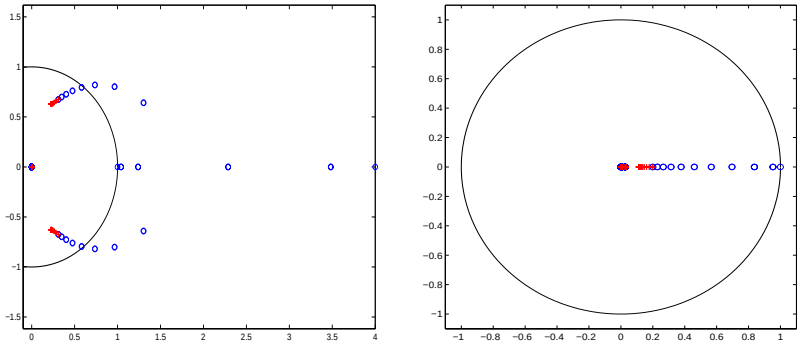

FIG. 4. *Eigenvalue spectra of* $\widehat{M^{REL}_{SGS}(\omega)}$ *for Baumann's DG method (without damping:* $\sigma = 1$, $\mu = 0$, $\alpha = 1$*) relative to the unit circle.*

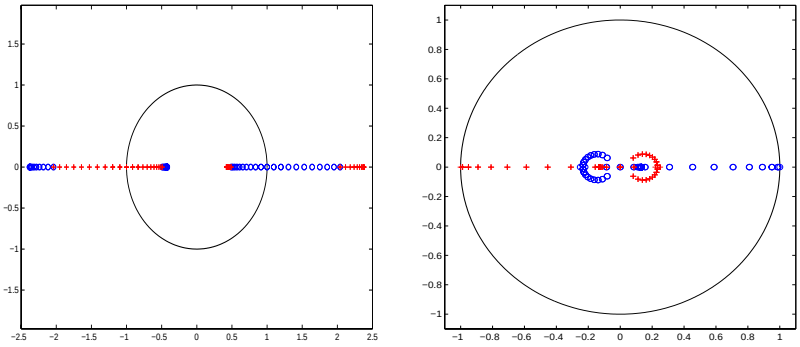

FIG. 5. *Eigenvalue spectra of* $\widehat{M^{REL}_{JOR}(\omega)}$ *for symmetric DG method (without damping:* $\sigma = -1$, $\mu = 0$, $\alpha = 1$*) relative to the unit circle.*

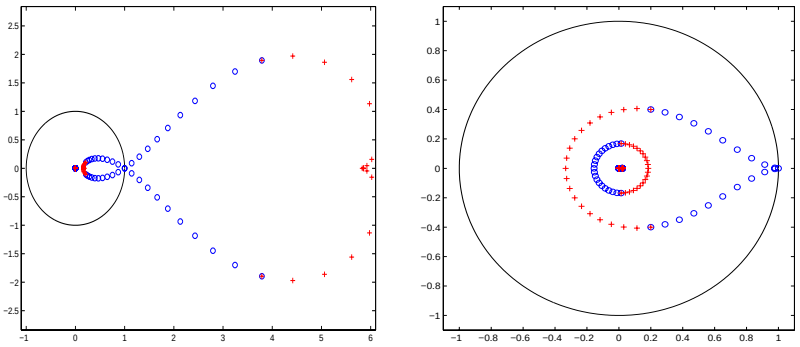

FIG. 6. *Eigenvalue spectra of* $\widehat{M^{REL}_{DGS}(\omega)}$ *for the symmetric DG method (without damping:* $\sigma = -1$, $\mu = 0$, $\alpha = 1$*) relative to the unit circle.*

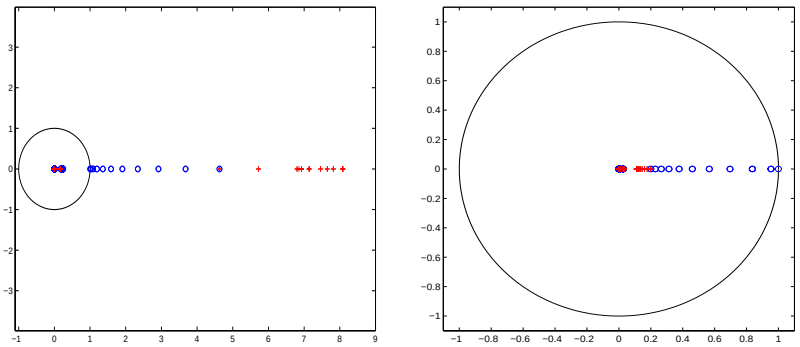

FIG. 7. *Eigenvalue spectra of* $\widehat{M^{REL}_{SGS}(\omega)}$ *for the symmetric DG method (without damping:* $\sigma = -1$, $\mu = 0$, $\alpha = 1$*) relative to the unit circle.*

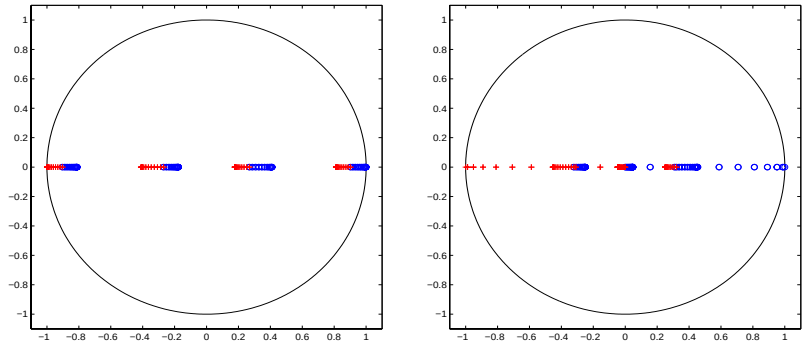

Cellwise order Pointwise order

$\circ : \omega_{low} \in [-\pi/2h, \pi/2h]; \;\; + : \omega_{high} \in [-\pi/h, -\pi/2h] \cup [\pi/2h, \pi/h]$

FIG. 8. *Eigenvalue spectra of* $\widehat{M^{REL}_{JOR}}(\omega)$ *for the IP method (without damping:* $\sigma = -1$, $\mu = 10/h$, $\alpha = 1$*) relative to the unit circle.*

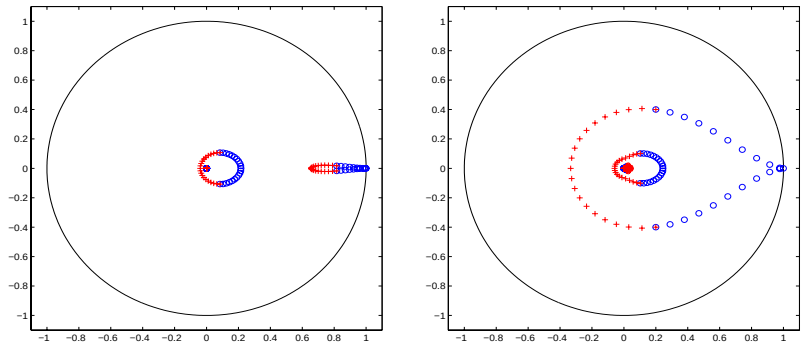

Cellwise order Pointwise order

$\circ : \omega_{low} \in [-\pi/2h, \pi/2h]; \;\; + : \omega_{high} \in [-\pi/h, -\pi/2h] \cup [\pi/2h, \pi/h].$

FIG. 9. *Eigenvalue spectra of* $\widehat{M^{REL}_{DGS}}(\omega)$ *for the IP method (without damping:* $\sigma = -1$, $\mu = 10/h$, $\alpha = 1$*) relative to the unit circle.*

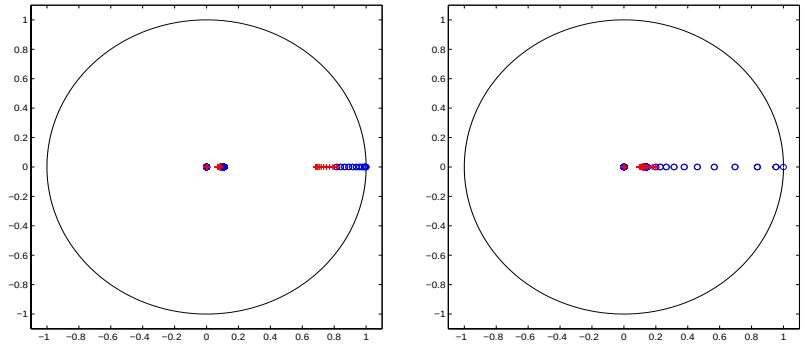

Cellwise order Pointwise order

$\circ : \omega_{low} \in [-\pi/2h, \pi/2h]; \;\; + : \omega_{high} \in [-\pi/h, -\pi/2h] \cup [\pi/2h, \pi/h]$

FIG. 10. *Eigenvalue spectra of* $\widehat{M^{REL}_{SGS}}(\omega)$ *for the IP method (without damping:* $\sigma = -1$, $\mu = 10/h$, $\alpha = 1$*) relative to the unit circle.*

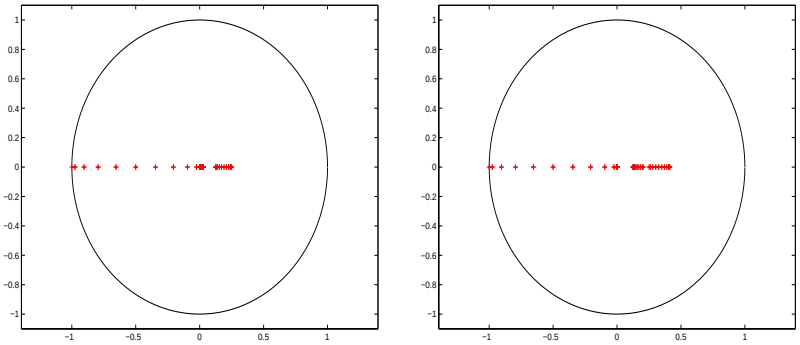

FIG. 11. *Eigenvalue spectra of* $\mathbf{FT}(M_{JOR}^{REL}(I_h - P_{hH}R_{Hh}))(\omega)$ *without damping* ($\alpha = 1$).

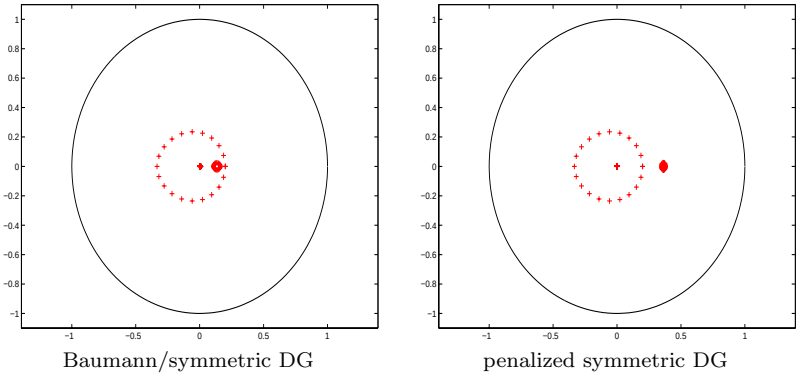

FIG. 12. *Eigenvalue spectra of* $\mathbf{FT}(M_{DGS}^{REL}(I_h - P_{hH}R_{Hh}))(\omega)$ *without damping* ($\alpha = 1$).

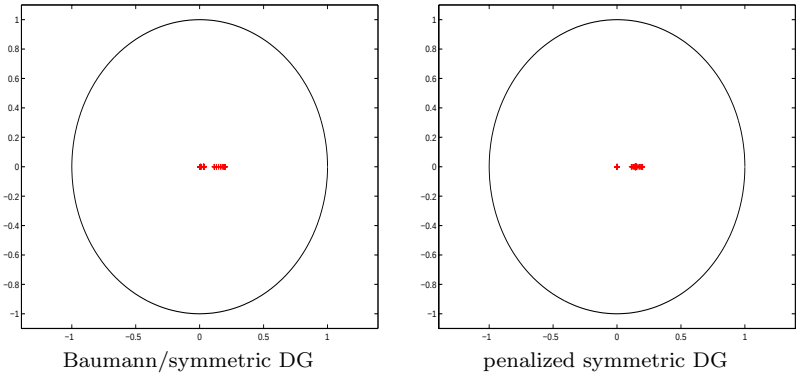

FIG. 13. *Eigenvalue spectra of* $\mathbf{FT}(M_{DGS_U}^{REL}(I_h - P_{hH}R_{Hh})M_{DGS_L}^{REL})(\omega)$ *without damping* ($\alpha = 1$).

In Table 4 we show the spectral radii for the corresponding operators $M_h^{\mathrm{REL}}(I_h - P_{hH}R_{Hh})$. For the spectral radius of symmetric damped Gauss-Seidel (DGS) the damping parameter for DGS is used. In the next section we use a similar approach to optimize the TLA.

TABLE 3
Damping parameters for the relaxation.

α	Baumann/symmetric DG	IP DG ($\mu = 10/h$)
JOR	8/11	0.773
DGS	15/16	1.024

TABLE 4
Spectral radii of $M^{REL}(I_h - P_{hH}R_{Hh})$ for damping parameters as in Table 3.

$\rho(M^{REL}(I_h - P_{hH}R_{Hh}))$	Baumann/symmetric DG	IP DG ($\mu = 10/h$)
JOR	0.455	0.591
DGS	0.250	0.365
Symm-DGS	0.203	0.200

5. Two-level analysis. In this section we study the convergence behavior of a TLA for both the error and the residue. In a fashion similar to how we determined relaxation parameters for the smoothing operators, we determine optimal relaxation parameters for the two-level operators in order to minimize the spectral radii. The amplification of the error for the TLA is given by the operator

$$\begin{aligned} M_h^{TLA} &= \left(M_h^{\mathrm{REL}}\right)^{\nu_2} M_h^{\mathrm{CGC}} \left(M_h^{\mathrm{REL}}\right)^{\nu_1} \\ &= \left(M_h^{\mathrm{REL}}\right)^{\nu_2} \left(I - P_{hH} L_H^{-1} \overline{R}_{Hh} L_h\right) \left(M_h^{\mathrm{REL}}\right)^{\nu_1}, \end{aligned}$$

where ν_1 and ν_2 are the number of pre- (post-) relaxation sweeps, respectively, and M_h^{CGC} is the amplification operator of the coarse-grid correction. The amplification operator for the residue is

$$\begin{aligned} \overline{M}_h^{TLA} &= (\overline{M}_h^{REL})^{\nu_2} \, \overline{M}_h^{CGC} \, (\overline{M}_h^{REL})^{\nu_1} \\ &= \left(L_h M_h^{\mathrm{REL}} L_h^{-1}\right)^{\nu_2} L_h M_h^{\mathrm{CGC}} L_h^{-1} \left(L_h M_h^{\mathrm{REL}} L_h^{-1}\right)^{\nu_1}. \end{aligned}$$

In section 2.4 we already noticed the Galerkin relation (2.11) between the discretization on the finer and the coarser grids and that, because test and trial spaces are the same, the residual restriction $\overline{R}_{Hh}$ is given by $\overline{R}_{Hh} = P_{hH}^T$, i.e., the adjoint of the prolongation. The consequence is that $M_h^{CGC} P_{hH} = 0$ for the solution and that $\overline{R}_{Hh} \overline{M}_h^{CGC} = 0$ for the residue. With the tools developed in the previous sections we now study the eigenvalue spectra of the two-level operators and their spectral norms.

5.1. Spectrum of the two-level iteration operator. The difference between the coarse-grid correction on the error and that on the residue is that the former splits an HF-error mode into an HF-mode and an LF-mode on the finer grid. This is in contrast to the coarse-grid correction on the residue, in which an LF-residual mode is split into an HF-mode and an LF-mode on the finer grid [14].

This implies that if we are interested in the error reduction, we should apply the smoothing operator M_h^{REL} *before* the coarse-grid correction. On the other hand, if we are interested in residue reduction we should apply the smoothing *after* the coarse-grid correction operator $\overline{M}_h^{CGC}$. Therefore, for the error, we are particularly interested in the behavior of the spectrum and the two-norm of

$$M_h^{\mathrm{CGC}} M_h^{\mathrm{REL}} = \left(I - P_{hH} L_H^{-1} \overline{R}_{Hh} L_h\right) M_h^{\mathrm{REL}},$$

whereas for the residue we want to study

$$\overline{M}_h^{REL} \, \overline{M}_h^{CGC} = \left(L_h M_h^{\mathrm{REL}} L_h^{-1}\right) \left(I - L_h P_{hH} L_H^{-1} \overline{R}_{Hh}\right).$$

TABLE 5
Spectral radii $\rho(M_h^{CGC}M_h^{REL}) = \rho(\overline{M}_h^{REL}\overline{M}_h^{CGC})$ *for optimal damping parameters.*

$\rho(M_h^{CGC}M_h^{REL})$	Baum DG	Symm DG	IP DG ($\mu = 10/h$)
$M_h^{CGC}M_{JOR}^{REL}$	0.401	0.314	0.422
$M_h^{CGC}M_{DGS}^{REL}$	0.220	0.143	0.189
$M_{DGS_U}^{REL}M_h^{CGC}M_{DGS_L}^{REL}$	0.119	0.073	0.139

TABLE 6
The spectral norm ($\sigma_{\max}$) *after one iteration for the residue with optimal damping.*

	$\overline{M}_h^{CGC}\overline{M}_{JOR}^{REL}$	$\overline{M}_h^{CGC}\overline{M}_{DGS}^{REL}$	$\overline{M}_{DGS_U}^{REL}\overline{M}_h^{CGC}\overline{M}_{DGS_L}^{REL}$
Baum DG	1.762	1.364	0.557
Symm DG	1.282	0.506	0.104
IP DG ($\mu = 10/h$)	1.518	0.699	0.301

It is clear that the spectra of these operators are the same, but the norms may be different. For different types of DG methods, viz. for Baumann's method ($\sigma = 1$, $\mu = 0$), the symmetric DG method ($\sigma = -1$, $\mu = 0$), and for the IP method ($\sigma = -1$, $\mu = C/h$), the spectra of the two-level operators can be studied as in section 4 for the smoothing operators. The spectral radii of the two-level operators are shown in Table 5.

We see that the two-level amplification operators for the symmetric DG method have the smallest spectral radii, which indicates that the final convergence rate will be faster, compared with the Baumann and IP DG methods.

5.2. Spectral norm of the iteration operator for the error and residue. From section 5.1 we know that all TLAs will converge rapidly after a sufficient number of iterations. However, since we want to minimize the total amount of iteration sweeps, we need to be sure also that the spectral norms of the iteration operators are sufficiently small. In order to check this we apply the singular value decomposition (SVD) to the Fourier transform of the amplification operators,

$$\mathbf{FT}\left(\left(M_h^{\mathrm{TLA}}\right)^t\right)(\omega) = U(\omega)\Sigma(\omega)V^T(\omega), \tag{5.1}$$

where, in view of our function basis, $U(\omega)$ and $V(\omega)$ are 8×8 unitary matrices and $\Sigma(\omega)$ is a real 8×8 diagonal matrix with singular values. The number of iterations is denoted by t. So, if we consider the error of the approximation, then according to (5.1), this error is first expressed on the basis $V(\omega)$, damped/amplified by $\Sigma(\omega)$, and then transformed to the basis $U(\omega)$. Since the spectral norm of the operator is the maximum singular value, this norm tells us how well the error (resp., the residue) is damped after t sweeps. The column of $V(\omega)$ determines the corresponding error/residual component.

The spectral norms after one iteration of the optimized two-level operators on the residue for the different types of DG methods are shown in Table 6. We see that not all two-level operators immediately converge. However, the situation changes if we look at the spectral norm of the two-level operators after two iterations (see Table 7). Then all methods converge, even by a significant factor. The spectral norms of the iteration operators on the error are the same as for the residual, except for Baumann's DG method. For this method the error-amplification norm becomes even unbounded (for vanishing frequency ω). This is related to the lack of adjoint consistency as

TABLE 7
The spectral norm ($\sigma_{\max}$) after two iterations for the residue with optimal damping.

	$\overline{M}_h^{CGC}\overline{M}_{JOR}^{REL}$	$\overline{M}_h^{CGC}\overline{M}_{DGS}^{REL}$	$\overline{M}_{DGS_U}^{REL}\overline{M}_h^{CGC}\overline{M}_{DGS_L}^{REL}$
Baum DG	0.684	0.447	0.064
Symm DG	0.403	0.083	0.007
IP DG ($\mu = 10/h$)	0.640	0.284	0.038

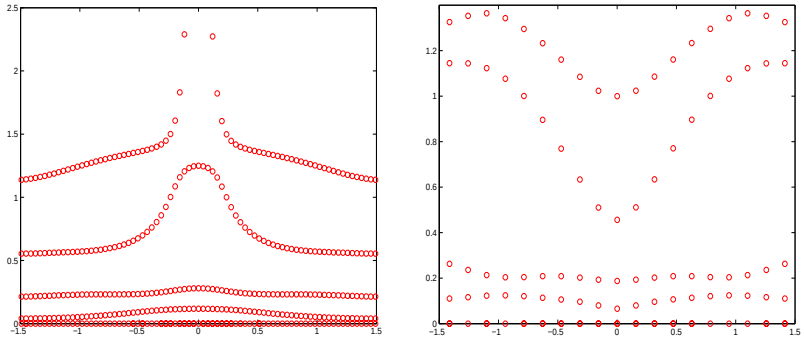

Baumann, $\widehat{M_h^{\mathrm{TLA}}}(\omega)$ Baumann, $\widehat{\overline{M}_h^{\mathrm{TLA}}}(\omega)$

FIG. 14. *Singular values $\Sigma(\omega)$, $\omega \in [-\pi/2, \pi/2]$, for a TLA iteration operator: $\widehat{M_h^{\mathrm{TLA}}}(\omega) = \widehat{M_h^{\mathrm{CGC}}}(\omega)\widehat{M_{\mathrm{DGS}}^{\mathrm{REL}}}(\omega)$ and $\widehat{\overline{M}_h^{\mathrm{TLA}}}(\omega) = \widehat{M_{\mathrm{DGS}}^{\mathrm{REL}}}(\omega)\widehat{M_h^{\mathrm{CGC}}}(\omega)$.*

indicated in [3]. We show the singular values of $\widehat{M_h^{\mathrm{TLA}}}(\omega)$ and $\widehat{\overline{M}_h^{\mathrm{TLA}}}(\omega)$ in Figures 14–16. We see that (as expected) in all cases four singular values vanish and that all singular values (except for $\widehat{M_h^{\mathrm{TLA}}}(\omega)$ for Baumann's method) are much smaller than one.

6. Galerkin relation and consistency. By the nature of the DG method, it is clear that the Galerkin relation,

$$L_H = \overline{R}_{Hh} L_h P_{hH} \,,$$

exists between the discrete operators on the fine grid and the coarse grid, provided that $\overline{R}_{Hh} = P_{hH}^T$ and that P_{hH} satisfies the requirement that $\mathbf{u}_h$ and $P_{hH}\mathbf{u}_H$ represent the same piecewise polynomial. For the prolongation introduced in section 2.4 this holds true by construction.

The Galerkin relation, the order of consistency, and the order of convergence are easily verified by Fourier analysis. In order to see this in detail and to compute the corresponding order constants, we show some results of this analysis, which also yields some additional insight with respect to the lack of adjoint consistency of Baumann's method (see [3]).

For the analysis we use the four functions in the basis (2.6) with $p = 2$ and consider the related pointwise stencil (2.9). First, we are interested in the truncation error operator

$$\tau_h = L_h R_h - \overline{R}_h L \tag{6.1}$$

and the operator corresponding to the discrete convergence, $C_h = L_h^{-1}\tau_h$. In (6.1) $R_h : C^1(\Omega_h) \to \mathbb{R}^{4\mathbb{Z}_h}$ is the injective restriction similar to (3.5), whereas the second

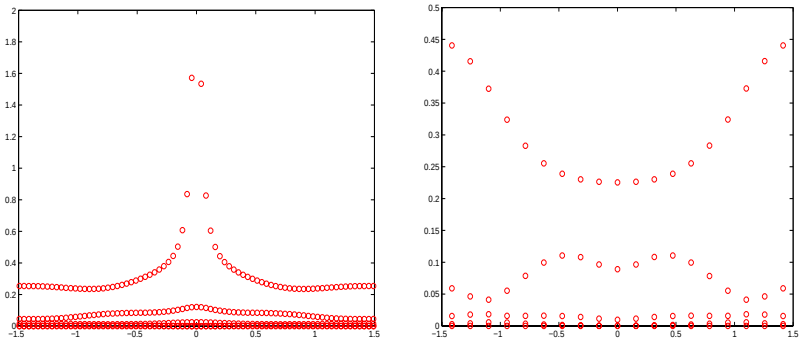

Baumann, $\widehat{\left(M_h^{\mathrm{TLA}}\right)^2}(\omega)$ Baumann, $\widehat{\left(\overline{M}_h^{\mathrm{TLA}}\right)^2}(\omega)$

FIG. 15. *Singular values* $\Sigma(\omega)$, $\omega \in [-\pi/2, \pi/2]$, *for two steps of the TLA-iteration operator.*

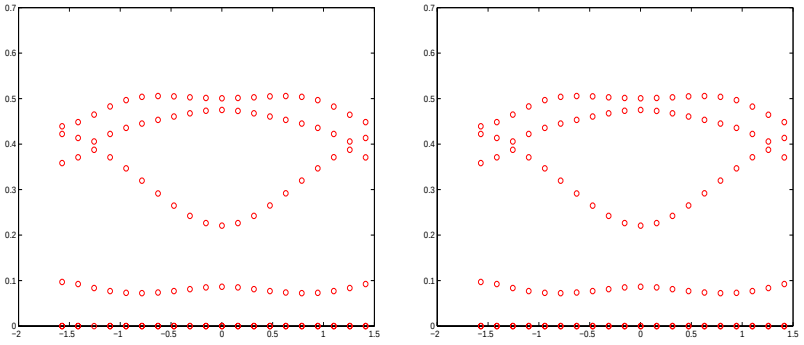

Symmetric DG, $\widehat{M_h^{\mathrm{TLA}}}(\omega)$ Symmetric DG, $\widehat{\overline{M}_h^{\mathrm{TLA}}}(\omega)$

FIG. 16. *Singular values* $\Sigma(\omega)$, $\omega \in [-\pi/2, \pi/2]$, *for one step of the symmetric DG TLA iteration operator.*

restriction is the Galerkin restriction $\overline{R}_h : C^1(\Omega_h) \to \mathbb{R}^{4\mathbb{Z}_h}$, defined such that for all $f \in C^1(\Omega_h)$,

$$\left(\overline{R}_h f\right)(jh) = \begin{bmatrix} \int_{(j-1)h}^{jh} \phi_k(x) f(x) dx, & k \in \{1,2\}, \\ \int_{jh}^{(j+1)h} \phi_k(x) f(x) dx, & k \in \{3,4\}, \end{bmatrix}$$

where ϕ_k are the basis functions in pointwise ordering. With $P_h : \mathbb{R}^{4\mathbb{Z}_h} \to \mathrm{Span}(\phi_{j,e}) \subset C^1(\Omega_h)$ the interpolation with $R_h P_h = I_h$, it is clear that, by construction, $P_h = P_{hH} P_H$ and $\overline{R}_H = \overline{R}_{Hh} \overline{R}_h$, and the discrete operator is characterized by $L_h = \overline{R}_h L P_h$. Hence, $L_H = \overline{R}_H L P_H = \overline{R}_{Hh} \overline{R}_h L P_h P_{hH} = \overline{R}_{Hh} L_h P_{hH}$. Furthermore, we write for the truncation error:

$$\tau_h e^{i\omega x} = \tau_h e_\omega(x) = (L_h R_h e_\omega - \overline{R}_h L e_\omega)(x).$$

Using (3.5) and the definition of $\overline{R}_h$, we find

$$\tau_h e_\omega = L_h e^{i\omega jh} \begin{bmatrix} 1 - e^{-i\omega h} - i\omega h \\ 1 \\ 1 \\ 1 - e^{i\omega h} + i\omega h \end{bmatrix} - \omega^2 h e^{i\omega jh} \begin{bmatrix} \int_0^1 e^{i\omega h(t-1)} t^2 (1-t) dt \\ \int_0^1 e^{i\omega h(t-1)} t dt \\ \int_0^1 e^{i\omega ht} (1-t) dt \\ \int_0^1 e^{i\omega ht} t (1-t)^2 dt \end{bmatrix},$$

TABLE 8

The expansion of (6.4) *for* $\omega h \to 0$*, i.e., the order of convergence: pointwise values* ($\widehat{v}_2$ *and* $\widehat{v}_3$) *and pointwise derivatives* ($\widehat{v}_1$ *and* $\widehat{v}_4$) *at the nodal points.*

Baumann	Symmetric	IP
$\sigma = 1$ $\mu = 0$	$\sigma = -1$ $\mu = 0$	$\sigma = -1$ $\mu = 1/h$
$\begin{pmatrix} \frac{1}{120}h^4\omega^4 + O(h^5\omega^5) \\ \frac{1}{840}h^4\omega^4 + O(h^5\omega^5) \\ \frac{1}{840}h^4\omega^4 + O(h^5\omega^5) \\ \frac{1}{120}h^4\omega^4 + O(h^5\omega^5) \end{pmatrix}$	$\begin{pmatrix} \frac{1}{120}h^4\omega^4 + O(h^5\omega^5) \\ \frac{1}{3360}h^5\omega^5 + O(h^6\omega^6) \\ \frac{1}{3360}h^5\omega^5 + O(h^6\omega^6) \\ \frac{1}{120}h^4\omega^4 + O(h^5\omega^5) \end{pmatrix}$	$\begin{pmatrix} \frac{1}{120}h^4\omega^4 + O(h^5\omega^5) \\ \frac{1}{2800}h^5\omega^5 + O(h^6\omega^6) \\ \frac{1}{2800}h^5\omega^5 + O(h^6\omega^6) \\ \frac{1}{120}h^4\omega^4 + O(h^5\omega^5) \end{pmatrix}$

where the basis functions are scaled to the master element $\widehat{\Omega} = [0, 1]$. Hence,

(6.2)
$$\tau_h e_\omega = \left(\widehat{L_h}(\omega) \begin{bmatrix} 1 - e^{-i\omega h} - i\omega h \\ 1 \\ 1 \\ 1 - e^{i\omega h} + i\omega h \end{bmatrix} - \omega^2 h \begin{bmatrix} \int_0^1 e^{i\omega h(t-1)} t^2(1-t)dt \\ \int_0^1 e^{i\omega h(t-1)} t dt \\ \int_0^1 e^{i\omega ht}(1-t)dt \\ \int_0^1 e^{i\omega ht} t(1-t)^2 dt \end{bmatrix} \right) e^{i\omega jh}$$
$$= \left(\widehat{L_h}(\omega)\widehat{R_h}(\omega) - \widehat{\overline{R}}_h(\omega)\widehat{L}(\omega) \right) e^{i\omega jh},$$

where $\widehat{L_h}(\omega)$ is the Fourier transform of the block-Toeplitz matrix L_h. Now we find the expansion of the truncation error for $h \to 0$ from (6.2). Both for Baumann's method ($\sigma = 1, \mu = 0$) and for the symmetric DG method without penalty ($\sigma = -1, \mu = 0$) and with IP ($\sigma = -1, \mu = 1/h$), (the absolute value of) the truncation error is

$$\tau e_\omega = \begin{bmatrix} \frac{1}{720}h^3\omega^4 + O(h^4\omega^5) \\ 0 \\ 0 \\ \frac{1}{720}h^3\omega^4 + O(h^4\omega^5) \end{bmatrix}. \tag{6.3}$$

Taking into account the factor h^{d-2}, typical for the FEM difference stencil (with $d = 1$ the dimension of cell Ω_e), we recognize in (6.3) the fourth order consistency of the discretization.

Similarly, we study the discrete convergence (where no such factor exists) by

$$C_h\, e_\omega = L_h^{-1}\tau_h\, e_\omega = \widehat{L_h}^{-1}(\omega) \left(\widehat{L_h}(\omega)\widehat{R_h}(\omega) - \widehat{\overline{R}_h}(\omega)\widehat{L}(\omega) \right) e^{i\omega jh}. \tag{6.4}$$

The results for the different methods are given in Table 8. We see that the symmetric DG methods, with and without IP, are more accurate with respect to the pointwise function values than Baumann's method. However, there is no difference in the order of accuracy with respect to the pointwise derivatives.

7. Numerical results. In this section we show by numerical experiments the convergence behavior of the two-level iteration operator for the error with the Baumann and symmetric DG methods for the smoothers JOR, DGS, and symmetric DGS with the optimal damping parameters. For this purpose we solve Poisson's equation

$$-u_{xx} = \frac{e^{x/\epsilon}}{\epsilon^2(\epsilon^{1/\epsilon} - 1)} \text{ with } u(0) = 0,\ u(1) = 0.$$

TABLE 9
Numerically obtained convergence factors corresponding to $\rho(M_h^{CGC}M_h^{REL}) = \rho(\overline{M}_h^{REL}\overline{M}_h^{CGC})$.

$\rho(M_h^{CGC}M_h^{REL})$	Baum DG	Symm DG
$M_h^{CGC}M_{JOR}^{REL}$	0.38	0.30
$M_h^{CGC}M_{DGS}^{REL}$	0.22	0.14
$M_{DGS_U}^{REL}M_h^{CGC}M_{DGS_L}^{REL}$	0.11	0.07

The choice of the right-hand side is unimportant, but starting with zero, in this example both low and high frequencies are present in the error. To obtain the discrete system we use the fourth order polynomial basis (1) and we set the meshwidth $h = 2^{-N}$. We start with an initial function $u_h^0 = u_{h,\mathrm{PRE}}^0$ on the finer grid. We apply ν_1 prerelaxation sweeps

$$u_{h,\mathrm{PRE}}^{i+1} = u_{h,\mathrm{PRE}}^{i} + B_h\left(f_h - L_h u_{h,\mathrm{PRE}}^{i}\right),$$

where B_h is an approximate inverse of L_h as given in Table 1. We update the solution by a coarse-grid correction step, solving the problem once on grid $H = 2^{1-N}$,

$$u_{h,\mathrm{POST}}^{0} = u_{h,\mathrm{PRE}}^{\nu_1} + P_{hH}L_H^{-1}\overline{R}_{Hh}(f_h - L_h u_{h,\mathrm{PRE}}^{\nu_1}),$$

and eventually we apply ν_2 postrelaxation sweeps,

$$u_{h,\mathrm{POST}}^{i+1} = u_{h,\mathrm{POST}}^{i} + B_h(f_h - L_h u_{h,\mathrm{POST}}^{i}),$$

to compute $u_h^{i+1} = u_{h,\mathrm{PRE}}^0 = u_{h,\mathrm{POST}}^{\nu_2}$. For the initial function u_h^0 we choose $u_h^0 = R_h u_0 = R_h \sin(2\pi/h)$. To show the convergence of the different methods we measure the residue in the vector norm (3.3). Hence we write

$$\|d_h\|_2 = \|f_h - L_h u_h\|_2 = \left(\sum_{e=1}^{64}\sum_{j=1}^{4} d_{he,j}^2\right)^{1/2},$$

Since the spectral radii of the two-level operators for the Baumann and symmetric DG methods calculated by Fourier analysis are smaller than those of the IP DG method, we only show results for the first two methods. The convergence of the residue for the two-level operator with different smoothers is shown in Figure 17.

We observe that both DG methods methods show immediately convergence, starting from the first iteration sweep. We see from Figure 17 and Table 9 that the spectral radii obtained from the numerical experiments coincide very well with spectral radii obtained by Fourier analysis (Table 5). We further remark that the symmetric DG method converges somewhat faster than Baumann's DG method. In spite of the phenomenon related to the lack of adjoint consistency of Baumann's method, the observed convergence of the error shows in practice the same behavior as the convergence of the residual.

8. Conclusion. In this paper we analyze the convergence of the MG algorithm for various DG methods. For convenience we restrict ourselves to the one-dimensional Poisson problem. We consider the (asymmetric) Baumann–Oden discretization and the symmetric DG discretization, with and without IP.

By the choice of a suitable basis in the space of the discontinuous piecewise polynomials that are used for the trial and test spaces, we are able to introduce a pointwise block-partitioning of the discrete operators. It appears that block-relaxation

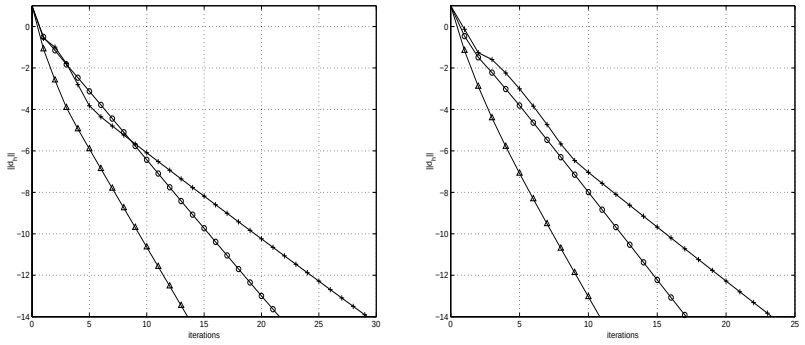

Baumann DG Symmetric DG

+: JOR; ∘: DGS; △: SGS.

FIG. 17. $\log(||d_h||_2)$ *as function of iterations for the two-level iteration operator on the error.*

methods based on this pointwise partitioning show completely different convergence properties from those found with classical, cellwise partitionings. Pointwise block-relaxations have much better convergence and smoothing properties. This is most significant for the symmetric DG discretization without IP. Here, cellwise block-Jacobi and block-Gauss–Seidel relaxations diverge, whereas the pointwise block-relaxations converge.

For the three discretization methods studied we compute optimal damping parameters for Jacobi, Gauss–Seidel, and SGS relaxations. The resulting smoothing factors lie between 0.6 (JOR for IP discretization) and 0.2 (symmetric DG). A two-level analysis with optimal damping parameter shows even better convergence: with spectral radius from 0.4 (JOR for IP discretization) to 0.075 (for symmetric GS and symmetric DG). An analysis of the spectral norm of the two-level amplification for the residue shows that a very small number of iteration steps (usually not more than two) is indeed sufficient to reduce the error by an order of magnitude.

The lack of adjoint consistency of Baumann's method and the resulting loss of accuracy for the solution (and *not* for its derivative) could be analyzed by means of Fourier analysis, and was also reflected in the spectral norm of the two-level amplification operator for the error.

REFERENCES

[1] M. ABRAMOWITZ AND I. A. STEGUN, *Handbook of Mathematical Functions*, Dover, New York, 1992.

[2] D. N. ARNOLD, *An interior penalty finite element method with discontinuous elements*, SIAM J. Numer. Anal., 19 (1982), pp. 742–760.

[3] D. N. ARNOLD, F. BREZZI, B. COCKBURN, AND L.D. MARINI, *Unified analysis of discontinuous Galerkin methods for elliptic problems*, SIAM J Numer. Anal., 39 (2002), pp. 1749–1779.

[4] C. E. BAUMANN AND J. T. ODEN, *A discontinuous hp-finite element method for convection diffusion problems,* Comput. Methods Appl. Mech. Engrg., 175 (1999), pp. 311–341.

[5] C. E. BAUMANN AND J. T. ODEN, *A discontinuous hp finite element method for convection-diffusion problems*, Comput. Methods Appl. Mech. Engrg., 175 (1999), pp. 311–341.

[6] C. E. BAUMANN, *An hp-Adaptive Discontinuous Finite Element Method for Computational Fluid Dynamics*, Ph.D. thesis, The University of Texas at Austin, Austin, TX, 1997.

[7] A. BRANDT, *Multi-level adaptive techniques (MLAT) for singular perturbation-problems*, in Numerical Analysis of Singular Perturbation Problems, P. W. Hemker and J. J. H. Miller, eds., Academic Press, New York, 1979, pp. 53–142.

[8] B. Cockburn, *Discontinuous Galerkin methods for convection-dominated problems*, in High-Order Methods for Computational Physics, T. Barth and H. Deconink, eds., Lecture Notes in Comput. Sci. Engrg. 9, Springer-Verlag, New York, 1999, pp. 69–224.

[9] L. Delves and C. Hall, *An implicit matching principle for global element calculations*, J. Inst. Math. Appl., 23 (1979), pp. 223–234.

[10] J. Gopalakrishnan and G. Kanschat, *A multilevel discontinuous Galerkin method*, Numer. Math., to appear.

[11] W. Hackbusch, *Multigrid Methods and Applications*, Springer-Verlag, Berlin, New York, 1985.

[12] P. W. Hemker, *Fourier Analysis of Gridfunctions, Prolongations and Restrictions*, Tech. report NW 93, Mathematical Centre, Amsterdam, 1980.

[13] P. W. Hemker, *On the structure of an adaptive multi-level algorithm*, BIT, 20 (1980), pp. 289–301.

[14] P. W. Hemker, *A note on defect correction processes with an approximate inverse of deficient rank*, Appl. Math. Comp., 8 (1982), pp. 137–139.

[15] P. W. Hemker and M. H. van Raalte, *Fourier Two-Level Analysis for Higher Dimensional Discontinuous Galerkin Discretisation*, Tech. report MAS-R0227, CWI, Amsterdam, 2002. Available online at http://db.cwi.nl/rappolten/index.php?jaar=2002&dept=13.

[16] P. Houston, C. Schwab, and E. Süli, *Discontinuous hp-Finite Element Methods for Advection-Diffusion Problems*, Tech. report 2000-07, ETHZ, Zürich, Switzerland, 2000.

[17] C. Johnson and J. Pitkäranta, *An analysis of the discontinuous Galerkin method for a scalar hyperbolic equation*, Math. Comp., 46 (1986), pp. 1–26.

[18] J. A. Nitsche, *Über ein Variationsprinzip zur Lösung Dirichlet-Problemen bei Verwendung von Teilräumen, die keinen Randbedingungen unterworfen sind*, Abh. Math. Sem. Univ. Hamburg, 36 (1971), pp. 9–15.

[19] J. T. Oden, I. Babuška, and C. E. Baumann, *A discontinuous hp finite element method for diffusion problems*, J. Comput. Phys., 146 (1998), pp. 491–519.

[20] W. H. Reed and T. R. Hill, *Triangular Mesh Methods for the Neutron Transport Equation*, Tech. report LA-UR-73-479, Los Alamos National Laboratory, Los Alamos, NM, 1973.

[21] B. Rivière, M. F. Wheeler, and V. Girault, *Improved energy estimates for interior penalty, constrained and discontinuous Galerkin methods for elliptic problems, Part* I, Comput. Geosci., 3 (1999), pp. 337–360.

[22] E. Süli, C. Schwab, and P. Houston, *hp-DGFEM for partial differential equations with non-negative characteristic form*, in Discontinuous Galerkin Methods. Theory, Computation and Applications, B. Cockburn, G. E. Karniadakis, and C.-W. Shu, eds., Lecture Notes in Comput. Sci. Engrg. 11, Springer-Verlag, New York, 2000, pp. 221–230.

[23] M. F. Wheeler, *An elliptic collocation-finite element method with interior penalties*, SIAM J. Numer. Anal., 15 (1978), pp. 152–161.